PHYSICAL REVIEW B

CONDENSED MATTER

Transport in polyaniline near the critical regime of the metal-insulator transition

Reghu Menon, C. O. Yoon, D. Moses, and A. J. Heeger

Institute for Polymers and Organic Solids, University of California at Santa Barbara, Santa Barbara, California 93106

Y. Cao

UNIAX Corporation, 5375 Overpass Road, Santa Barbara, California 93111

(Received 19 April 1993)

Critical behavior of the electrical conductivity near the disorder-induced metal-insulator (MI) transition has been observed in polyaniline (PANI) doped with camphor sulfonic acid (CSA). The temperature dependence of the resistivity (ρ) depends on the degree of disorder present in the PANI-CSA films. In the most metallic samples the resistivity is nearly temperature independent; whereas in the critical region of MI transition, $\rho(T)$ is characterized by a power-law temperature dependence, $\rho(T) \propto T^{-\beta}$. Resistivity ratios $\rho(1.4 \text{ K})/\rho(300 \text{ K})$ as low as 1.6 have been observed in the most metallic samples of PANI-CSA. In the metallic regime, the conductivity is characterized by $\sigma(T) = \sigma(0) + mT^{1/2}$ at low temperatures; the dependence of $m(H)$ on magnetic field provides information on the role of electron-electron interactions in the transport near the MI transition. The T^{-1} dependence found for inelastic-scattering time (τ_{in}) is in agreement with that predicted for metallic systems near the MI transition. For the samples initially in the critical regime, a magnetic field of 8–10 T induces the transition to variable-range hopping. The typical localization length in PANI-CSA just on the insulating side of the MI transition is about 80–130 Å. The magnitude of the positive magnetoresistance increases considerably as the system moves from the metallic to the insulating regime. The magnitude and quasilinear temperature dependence of the thermopower near the critical regime of the MI transition is typical of that expected for a metal.

I. INTRODUCTION

Heavily doped conjugated polymers exhibit many properties characteristic of the metallic state, including relatively high electrical conductivity, Pauli temperature independent magnetic susceptibility, linear term in the specific heat, absorption throughout the infrared with no energy gap, etc. Except for a few systems,[1,2] however, these highly conducting polymers typically do not exhibit the traditional signatures of metallic transport: (i) Resistivity (ρ) with a positive temperature coefficient, $d\rho/dT > 0$; (ii) thermoelectric power (S) proportional to the temperature. In recent years, the quality of pristine conjugated polymers has improved substantially; however, the doping process often results in inhomogeneity or even phase-segregated regions with large differences in the doping level. When processed from solution or synthesized by means of a precursor route, the conjugated macromolecular chains are often disordered and structurally amorphous. Although specific systems are partially crystalline, the residual amorphous regions can dominate the transport. Consequently, the characteristic metallic features in the bulk transport properties are severely limited by strong disorder.

The existence of partially filled bands implies that the electronic structure of heavily doped polymers will be that of a metal. It is well known, however, that disorder can result in localization of states; if the magnitude of the disorder potential is large compared with the bandwidth, all states become localized, and the system will be an insulator. In such an insulator, however, there is no gap in the density of states; the insulating properties result since the Fermi level (E_F) lies in an energy interval in which all states are localized—the system is a Fermi glass. In a Fermi glass, the conductivity is activated; at high temperatures the activation energy is a measure of the energy difference between E_F (which lies in the region of localized states) and the mobility edge; at lower temperatures, variable-range-hopping transport results from the existence of unoccupied localized electronic states near E_F. The metal-insulator (MI) transition occurs when the disorder is sufficiently weak that the mobility edges move away from the center of the band toward the band tails such that E_F lies in a region of extended states.

For each specific conducting polymer, it is important to quantify the disorder and to establish where the ma-

terial is in parameter space relative to the MI transition. Armed with such information, the polymer scientist can develop a realistic strategy for improving the material to the point where genuine metallic transport can be observed.

Recently, progress in the improvement of the electronic properties of conducting polyaniline (PANI) has been made by doping with functionalized sulfonic acids.[3,4] By using surfactant counterions, PANI has been made soluble in common organic solvents, in the conducting emeraldine salt form. As a result, solution processing of this conducting polymer has greatly improved the homogeneity of solid films (cast from solution), resulting in significant reduction in the extent of disorder. Because of these improvements, it is possible to begin to observe the intrinsic metallic features in bulk transport property measurements.[4]

The lowest value of the resistance ratio, $\rho_r = \rho(1.4 \text{ K})/\rho(300 \text{ K})$, that has been reported for iodine doped oriented polyacetylene[5] (with room-temperature conductivity of $\sim 10^5$ S/cm) is $\rho_r = 2.8$. In spite of the fact that the maximum room-temperature conductivity of PANI doped by $(\pm)$-10 camphor sulfonic acid (CSA) is smaller by more than two orders of magnitude (200–400 S/cm), resistivity ratios for PANI-CSA samples in the metallic regime are as small as $\rho_r = 1.6$. Moreover, the resistivity of PANI-CSA shows a positive temperature coefficient between 400 and 180 K; the resistivity decreases with decreasing temperature, as in a true metal.

The typical room-temperature conductivities for PANI-CSA films are about 200–400 S/cm, comparable to Mott's minimum metallic conductivity.[4] All the PANI-CSA samples show a temperature-independent Paul susceptibility (χ_p) for temperatures above approximately 50 K; the room-temperature values are $\chi_p = 2 \times 10^{-5}$ emu/mol-two rings.[6,7] Moreover, at low temperatures (~ 4 K), the Curie contribution due to the localized spins is significantly lower than for PANI doped by conventional protonic acids.[8] The room-temperature thermopower values for the PANI-CSA films are 10 ± 2 μV; the thermopower increases approximately linearly with the temperature.[9]

We present the results of a comprehensive study of the transport in PANI-CSA; we have observed three distinct types of behavior for PANI-CSA films: metallic, critical, and insulating, depending on the extent of disorder created in the material while processing the films. In the metallic regime the electron-electron interactions contribute to the conductivity and magnetoconductivity, at low temperatures. The power-law temperature dependence of $\rho(T)$ in PANI-CSA corresponds to the critical behavior near the Anderson MI transition.[10] Magnetic fields of 8–10 T induce a transition from the critical regime of MI transition to the insulating region where the states near E_F are localized and the transport takes place via variable-range hopping. PANI-CSA samples can be made with reduced disorder; such samples have properties indicating that the material has crossed the MI boundary onto the metallic regime. For PANI-CSA, the thermopower exhibits the linear temperature dependence characteristic of "metallic" behavior.

II. EXPERIMENT

PANI-CSA was prepared by mixing the emeraldine base with camphor sulfonic acid in agate mortar and pestle; the materials were handled in a glove bag filled with nitrogen.[3] All the PANI-CSA samples were prepared with a molar ratio of CSA to a phenyl-nitrogen repeat unit of 0.5. The PANI-CSA complex is soluble in various organic solvents. For the experimental studies reported here, the solutions were prepared by adding an appropriate quantity of PANI-CSA to meta-cresol. The mixture was stirred in an ultrasonic bath for 48 h and subsequently centrifuged.[3] Free-standing films of PANI-CSA were obtained by casting onto a glass plate and subsequently drying in air for 24 h on a hot plate at 50 °C. Film thicknesses were typically 10–50 μm. The films appeared isotropic in all respects.

The sample preparation conditions and the protonation level for all the PANI-CSA samples used in this experimental study are more or less identical. However, the subtle changes in morphology and crystallinity in the films are very dependent on factors like the concentration of the solution from which the films are cast, the rate of evaporation of the solvent, the thickness of the film, etc. Although the room-temperature conductivities of PANI-CSA films are not very affected by such details of the film-casting process, the low-temperature transport properties are quite sensitive to these factors. Slight differences in doping level could play a role; however, all samples were carefully prepared with a molar ratio of CSA to phenyl-nitrogen repeat unit of 0.5. Moreover, the fact that the room temperature values are not affected suggests that variations in doping level and/or deviations from stoichiometry are not significant. Scanning electron micrographs show no major differences in morphology in the various films, up to 0.1-μm resolution. Thus, the observed differences in the transport result from microscopic (molecular scale to nanoscale) changes in the disorder.

Four-terminal dc resistivity and magnetoresistance measurements were carried out using a computer-controlled automated measuring system. Electrical contacts were made with conducting graphite adhesive. To avoid sample heating at low temperatures, the current source was adjusted at each temperature so that the power dissipated into the sample was less than 1 μW. The linearity was checked by measuring voltage versus current, and the resistivity was obtained from the slope of the straight line. Temperature was measured with a calibrated platinum resistor (300–40 K) or a calibrated carbon-glass resistor (40–1.2 K) by a temperature controller driven by the computer.

The differential technique was used for the thermopower measurements.[11] Two isolated copper blocks were alternatively heated and the heating current was accurately controlled by computer. The temperature difference between the two copper blocks was measured by a chromel-constantan thermocouple and did not exceed 0.5 K at each thermal cycle. In each thermopower experiment, five samples were placed across the copper blocks using pressure contacts to ensure excellent thermal and electrical contacts at low temperatures. The

voltage difference across the samples was averaged for one complete thermal cycling, after equilibrating at each specified temperature. The temperature gradient from the thermocouple to sample was calibrated for the entire range of temperature, and the absolute thermoelectric power (TEP) of the sample was obtained by subtracting the TEP of copper wire, which was calibrated against the absolute TEP scale for lead.[12] All the parameters during the experiment were controlled by computer.

III. RESULTS AND DISCUSSION

A. Temperature dependence of the resistivity

The transport properties of the PANI-CSA films can be classified in three groups according to the resistivity ratio $\rho_r = \rho(1.4 \text{ K})/\rho(300 \text{ K})$: (i) Metallic side of the MI transition; (ii) critical regime of the MI transition; (iii) insulating side of the MI transition. On the metallic side of the MI transition, $\rho_r < 2$; in the critical regime, $2 < \rho_r < 6$; and on the insulating side of the MI transition, $\rho_r > 6$. To explicitly characterize the three regimes, we define the reduced activation energy,

$$W = -T\frac{d \ln\rho(T)}{dT} , \qquad (1)$$

and plot W versus temperature.[13] The results for PANI-CSA are summarized in Fig. 1. For samples on the metallic side of the MI transition, W decreases upon decreasing the temperature below 40 K, whereas for samples in the critical regime, W is constant from 40 to 1.4 K. On the insulating side of the MI transition, W increases as the temperature is lowered.

For a three-dimensional (3D) conductor close to the MI transition, the correlation length (L_c) is large and has a power-law dependence on $\delta = [|E_F - E_c|/E_c] < 1$; $L_c \approx a\delta^{-1/\nu}$, where a is a microscopic length, ν is the critical exponent, E_F is the Fermi energy, and E_c is the mobility edge.[10] In this critical region, Larkin and

FIG. 1. Log-log plot of $W(T)$ vs temperature for PANI-CSA in the metallic (●), critical (▲), and insulating (♦) regimes. In the critical regime, $W = \beta$ [see Eq. (2)]; in the VRH regime, $W(T) = \frac{1}{4}(T_0/T)^{1/4}$.

Khmelnitskii[10] found that the resistivity is not activated, but follows a power law as a function of temperature,

$$\rho(T) \approx \left[\frac{e^2 p_F}{\hbar^2}\right]\left[\frac{k_B T}{E_F}\right]^{-1/\eta} \propto T^{-\beta} , \qquad (2)$$

where p_F is the Fermi momentum, e is the electron charge, and $1 < \eta < 3$. Thus, in the critical regime [from Eq. (1)], $W = \beta = 1/\eta$. As shown in Fig. 1, W is constant for samples in the critical regime (the solid line through the data has slope zero), with values for β typically falling in the range $0.26 < \beta < 0.4$.

When the Fermi energy lies in a region of localized states, the system is a Fermi glass insulator, and the low-temperature transport is by variable-range hopping (VRH). For VRH in 3D,

$$\rho(T) = \rho_0 \exp[(T_0/T)^{1/4}] , \qquad (3)$$

where

$$T_0 = 16/k_B N(E_F)L_c^3 , \qquad (4)$$

k_B is the Boltzmann constant, $N(E_F)$ is the density of states at the Fermi level, and L_c is the localization length.[14] Thus, for VRH [from Eq. (1)], $W(T) = \frac{1}{4}(T_0/T)^{1/4}$, in agreement with the data presented in Fig. 1 (the solid line through the data has slope 0.25).

The temperature dependence of $\rho(T)$ on the metallic side of the MI transition is shown in greater detail in Fig. 2(a). Although $\rho(T)$ increases at low temperature, the temperature dependence is extremely weak; the system has crossed over from the power-law dependence characteristic of the critical regime to "metallic" behavior. Application of an 8-T external magnetic field increases the low-temperature resistivity [Fig. 2(a)]. In an external magnetic field of 8 T, the temperature dependence approaches closer to the power-law regime, implying that the external field moves the system toward the critical regime ($\delta \rightarrow 0$). Nevertheless, even for $H = 8$ T, the log-log plot shows some residual curvature. The effects of localization and interaction on conductivity and magnetoconductance in the "metallic" regime is discussed in detail in Sec. III B.

The power-law dependence of Eq. (2) is universal and requires only that the disordered system be close to the MI transition, i.e., in the critical region where $\delta \ll 1$. The power-law temperature dependence, $\rho(T) \propto T^{-0.36}$, has been reported previously for PANI-CSA;[4] however, the crossover from the critical regime of the MI transition into the metallic regime (see Fig. 1) was not observed in the earlier measurements. The power-law temperature dependence of $\rho(T)$ has also been reported for doped polyacetylene and for doped polypyrrole;[5] however, the critical regime of the MI transition in conducting polymers was not explicitly identified previously.

The temperature dependence of resistivity for samples in the critical region of the MI transition is shown in Fig. 2(b). Over a wide temperature range (1.4–40 K), the resistivity follows a power-law dependence as predicted for the critical regime. Two examples are shown in Fig.
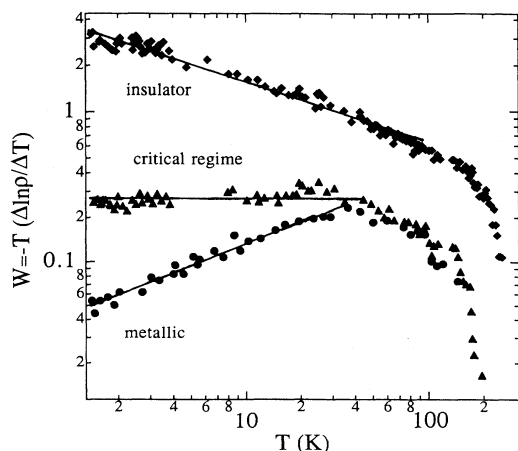
2(b), $\rho(T) \propto T^{-0.26}$ (●) where $\eta = 3.8$, and $\rho(T) \propto T^{-0.36}$ (■) where $\eta = 2.8$. The linearity on the log-log plot over the temperature range from 1.4 to 40 K demonstrates that $\rho(T,0) = \rho_{0m}(T/T_{0m})^{-\beta}$, where ρ_{0m} and T_{0m} are constants. The sample-to-sample variation of the exponent correlates with the resistivity ratio; samples with smaller (larger) ρ_r give smaller (larger) β. The temperature range over which the dependence is a power law is wider for samples with smaller $|\beta|$. A value of $\eta > 3$ indicates that the system is just entering into the metallic side of the MI transition from the critical regime. Although $\eta = 3.8$ is slightly above the theoretical limit for the power-law dependence, values for η as large as 4.5 have been reported for n-doped germanium in the critical regime of the MI transition.[13] Application of an 8-T magnetic field increases the resistivity; for $H = 8$ T, the temperature dependence is stronger than that of a power law [see Fig. 2(b)].

Assuming the resistivity in zero magnetic field follows Eq. (2) with $\eta \approx (0.36)^{-1} = 2.77$, one can compare the prefactor with that obtained from the measurements. Using $p_F = \hbar k_F$ and $k_F \approx \pi/2c$, the prefactor is given by $\rho_{0m} \approx e^2 p_F / \hbar^2 \approx 2 \times 10^{-4}$ Ω cm. From the data in Fig.

2(b) [with $E_F \approx 1$ eV in Eq. (2)], we obtain $\rho_{0m} \approx 6 \times 10^{-4}$ Ω cm, in approximate agreement with the theoretical value.

An example of the $\ln\rho$ vs $T^{-1/4}$ plot, appropriate for samples on the insulating side of the MI transition, is shown in Fig. 3. In Fig. 3(a), $\rho_r \approx 10^3$, and $T_0 \approx 3 \times 10^4$ K. For samples closer to the MI transition from the insulating side, VRH transport is observed as shown in Fig. 3(b), but with $\rho_r \approx 12$ and $T_0 \approx 230$ K.[4] Since the temperature dependence of the resistivity is characteristic of variable-range hopping, the states near the Fermi energy are localized. The $\ln\rho$ vs $T^{-1/4}$ plots for the normalized
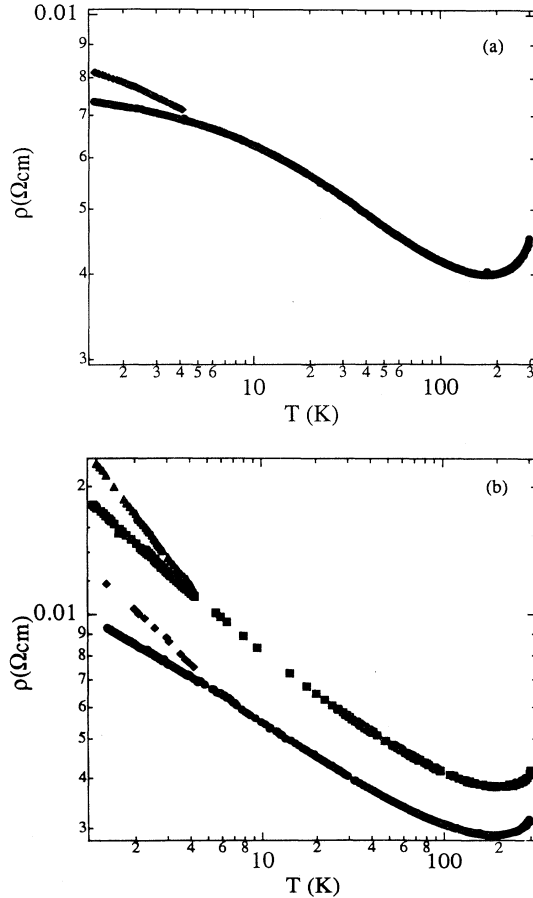

FIG. 2. Log-log plots of the resistivity of PANI-CSA. (a) Metallic regime, $H = 0$ T (●) and $H = 8$ T (◆); (b) critical regime, $[\rho(T) \propto T^{-0.26}]$, $H = 0$ T (●), and $H = 10$ T (◆); and $[\rho(T) = T^{-0.36}]$, $H = 0$ T (■), and $H = 8$ T (▲).
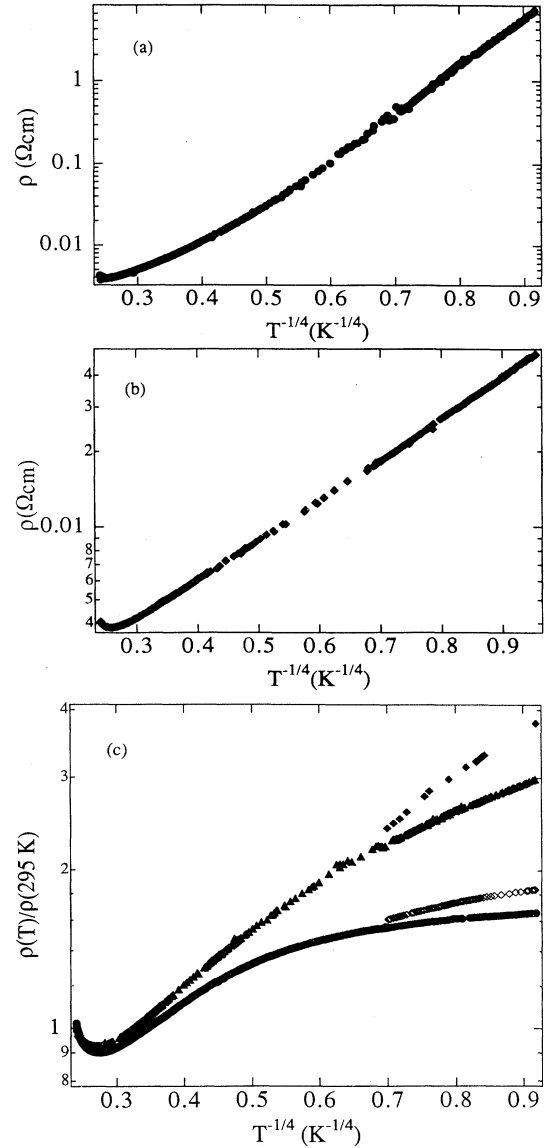

FIG. 3. $\rho(T)$ vs $T^{-1/4}$ for PANI-CSA in the insulating regime. (a) Data replotted for (◆) from Fig. 1. $T_0 = 2.9 \times 10^4$ K. (b) Insulating sample close to the MI transition, $T_0 = 230$ K. (c) Normalized resistivity vs $T^{-1/4}$ for PANI-CSA in the metallic regime, $H = 0$ T (●) and $H = 8$ T (◇); critical regime: $[\rho(T) \propto T^{-0.26}]$, $H = 0$ T (▲), and $H = 10$ T (◆).

resistivity of the samples on the metallic side (●) of the MI transition and in the critical regime for $\rho(T) \propto T^{-0.26}$ (▲) are shown in Fig. 3(c). The curvature is unambiguous. In both cases, however, the external magnetic field tends to localize the electronic states. A more detailed discussion of the magnetic-field dependence is given in Sec. III C.

B. Temperature dependence of the magnetoconductance in the "metallic" regime

The quantum corrections to the conductivity and the magnetoconductivity due to localization and electron-electron interactions have been extensively studied in disordered metals close to the MI transition.[15] The temperature dependence of the conductivity is given by the following expression:

$$\sigma(T) = \sigma(0) + mT^{1/2} + BT^{p/2} , \tag{5}$$

where the second term ($T^{1/2}$) results from thermally induced electron diffusion through states near the Fermi energy (reduced by electron-electron scattering), and the third term is the correction to the zero-temperature conductivity due to localization effects.[15] The value of p is determined by the temperature dependence of the scattering rate [$\tau^{-1} \propto T^p$] of the dominant dephasing mechanism. For electron-phonon scattering, $p = 3$; for inelastic electron-electron scattering, $p = 2$ and 1.5 in the clean and dirty limits, respectively. However, Belitz and Wysokinski[16] have shown that very near the MI transition, electron-electron scattering also leads to $p = 1$. The coefficient of the second terms is given by[15]

$$m = \alpha[\tfrac{4}{3} - \gamma(3F_\sigma/2)] , \tag{6a}$$

where

$$\alpha = (e^2/\hbar)(1.3/4\pi^2)(k_B/2\hbar D)^{1/2} , \tag{6b}$$

D is the diffusion constant, and γF_σ is the interaction parameter. Note, however, that since the screening length becomes very large near the MI transition, F_σ is expected to decrease toward zero.[15] Thus, in the metallic regime near the MI transition, $m \approx 4\alpha/3$. The expression for $\sigma(T)$ in the presence of magnetic field is given by

$$\sigma(H, T) = \sigma(H, 0) + m(H)T^{1/2} . \tag{7}$$

At fields sufficiently high that $g\mu_B H \gg k_B T$,

$$\sigma(H, T) = \sigma(H, 0) + \alpha[\tfrac{4}{3} - \gamma(F_\sigma/2)]T^{1/2} \tag{8}$$

assuming that α, γ, and F_σ are not dependent on the magnetic field.[17]

The extremely weak temperature dependence of the resistivity ($\rho_r = 1.6$) and the positive temperature coefficient of W below 40 K [as shown in Figs. 1 and 2(a)] are characteristic of PANI-CSA samples in the metallic regime. The temperature dependence of the conductivity of the sample with $\rho_r = 1.6$ is plotted vs $T^{1/2}$ in Figs. 4(a) and 4(b). The $T^{1/2}$ dependence is in agreement with Eq. (5), and consistent with metallic behavior near the MI transition [since the $T^{1/2}$ dependence implies that $p = 1$ in Eq. (5), we simply redefine α and γ to include B]. The data yield $\sigma(T) = \sigma(0) + mT^{1/2}$ with $m(0) = 10.8$
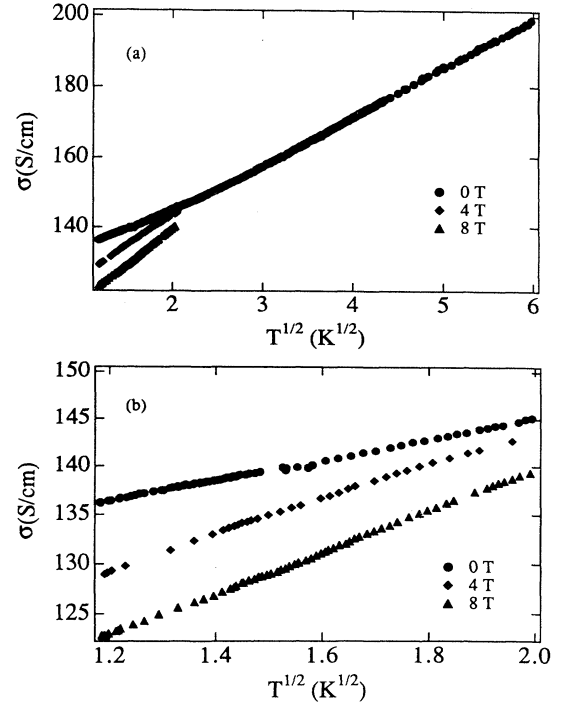

FIG. 4. (a) $\sigma(T)$ vs $T^{1/2}$ for PANI-CSA in the metallic regime at $H = 0$, 4, and 8 T. (b) Data below 4.2 K are shown on an expanded scale.

$S \, cm^{-1} \, K^{-1/2}$. In Figs. 4(a) and 4(b), we plot $\sigma(T)$ vs $T^{1/2}$ for $H = 0$, 4, and 8 T. The magnetic field decreases the low-temperature conductivity (positive magnetoresistance). At low temperatures [shown in greater detail in Fig. 4(b)], the slope of σ vs $T^{1/2}$ is field dependent, as predicted by Eqs. (6) and (7).

The parameters α and γF_σ can be estimated by using Eqs. (6a) and (7) for the values of $m(H)$ obtained at $H = 0$ and 8 T, respectively (note that for $T < 8$ K, $g\mu_B H > k_B T$). From Fig. 4,

$$\alpha[\tfrac{4}{3} - \gamma(3F_\sigma/2)] \approx 10.8 \; S \, cm^{-1} \, K^{-1/2} ,$$

$$\alpha[\tfrac{4}{3} - \gamma(F_\sigma/2)] \approx 19.8 \; S \, cm^{-1} \, K^{-1/2} .$$

The corresponding values for α and γF_σ are $\alpha \approx 18.3$ and $\gamma F_\sigma \approx 0.5$. This relatively small value for γF_σ is comparable to that found in studies of doped semiconductors at doping levels near the MI transition.[17] The magnetic field decreases the zero-temperature conductivity (negative magnetoconductance) and increases the slope of σ vs $T^{1/2}$; both effects result directly from electron-electron interactions and arise predominantly from the Zeeman splitting of the spin-up and spin-down bands.[15]

The magnetoconductance $\Delta\Sigma(H, T) = \sigma(H, T) - \sigma(0, T)$ is plotted vs magnetic field in Fig. 5. The conductivity is weakly field dependent at low fields (below 1 T) and then decreases with field. These data are replotted in Figs. 6(a) and 6(b); Fig. 6(a) presents $\Delta\Sigma(H, T)$ vs H^2 and Fig. 6(b) presents $\Delta\Sigma(H, T)$ vs $H^{1/2}$.

The contribution to $\Delta\Sigma(H, T) = \sigma(H, T) - \sigma(0, T)$ from
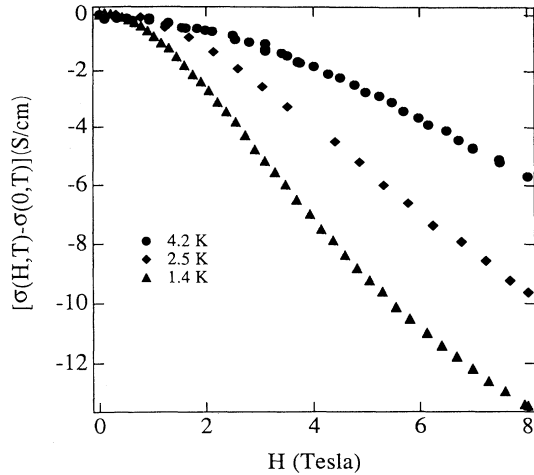
FIG. 5. Magnetoconductance vs H for PANI-CSA in the metallic regime at 4.2, 2.5, and 1.4 K.

electron-electron interactions can be written as follows:[17]

$$\Delta\Sigma_I(H,T)=-0.041\alpha(g\mu_B/k_B)^2\gamma F_\sigma T^{-3/2}H^2$$

$$(g\mu_B H \ll k_B T) , \quad (9a)$$

$$\Delta\Sigma_I(H,T)=\alpha\gamma F_\sigma T^{1/2}-0.77\alpha(g\mu_B/k_B)^{1/2}\gamma F_\sigma H^{1/2}$$
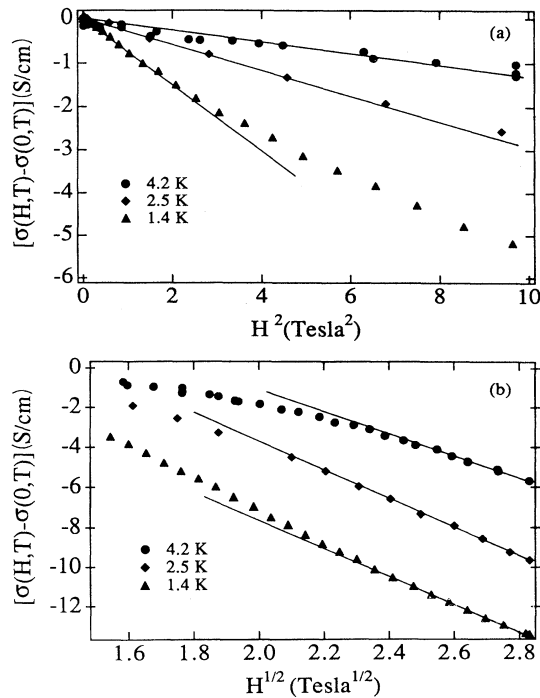
$$(g\mu_B H \gg k_B T) . \quad (9b)$$

FIG. 6. (a) Magnetoconductance vs H^2 for PANI-CSA in the metallic regime at 4.2, 2.5, and 1.4 K; the solid lines indicate H^2 dependence. (b) Magnetoconductance vs $H^{1/2}$ for PANI-CSA in the metallic regime at 4.2, 2.5, and 1.4 K; the solid lines indicate $H^{1/2}$ dependence.

At low and high fields, $\Delta\Sigma_I(H,T)$ is proportional to H^2 and $H^{1/2}$, respectively. The data summarized in Figs. 6(a) and 6(b) are in agreement with Eqs. (9a) and (9b).

For small magnetic fields, we follow Rosenbaum et al.[18] and Dai, Zhang, and Sarachik[17] and assume that the contributions to $\Delta\Sigma(H,T)$ which arise from electron-electron interactions and from "antilocalization" (due to spin-orbit scattering[19,20]) are additive. Thus, the total low-field magnetoconductance is given by

$$\Delta\Sigma(H,T)=-0.041\alpha(g\mu_B/k_B)^2\gamma F_\sigma T^{-3/2}H^2$$

$$-(1/48\pi^2)(e/c\hbar)^2 G_0(l_{in})^3 H^2 . \quad (10)$$

The second term on the right-hand side is the contribution due to antilocalization at weak fields; $G_0=(e^2/\hbar)$ and L_{in} is the inelastic-scattering length. The first term on the right-hand side can be estimated by using the values for α and γF_σ obtained above. Then, using the slope of $\Delta\Sigma$ vs H^2 [see Fig. 6(a)] the second term can be estimated. In this way, the value of the inelastic-scattering length can be calculated at each temperature. The results are shown in Fig. 7; l_{in} is inversely proportional to the square root of the temperature.

The inelastic-scattering time (τ_{in}) can be estimated from l_{in} with the relation $\tau_{in}=(l_{in})^2/D$; since $l_{in} \propto T^{-1/2}$, $\tau_{in} \propto T^{-1}$. The value of D calculated from Eq. (6b) (using the known value of $\alpha=18.3$) is $D\approx1.25\times10^{-2}$ cm^2 sec^{-1}. We conclude, therefore, that at 4.2 K, $\tau_{in}\sim10^{-10}$ sec, which is the same as that reported for potassium-doped polyacetylene[21] and various other amorphous metals.[22] The T^{-1} temperature dependence of τ_{in} is in agreement with the theoretical prediction of Belitz and Wysokinski[16] for the systems very close to the MI transition. The same T dependence of τ_{in} has been observed in metallic Si:B near the MI transition.[17]

C. Magnetic-field dependence of $\rho(H,T)$ in the critical and insulating regimes

Khmelnitskii and Larkin used scaling arguments to demonstrate that in the metallic region near the MI transition, the mobility edge can be shifted by an external magnetic field.[23] When the magnetic length $L_H=(\hbar c/eH)^{1/2}$ becomes comparable to L_c, the field causes the mobility edge (E_c) shift proportional to
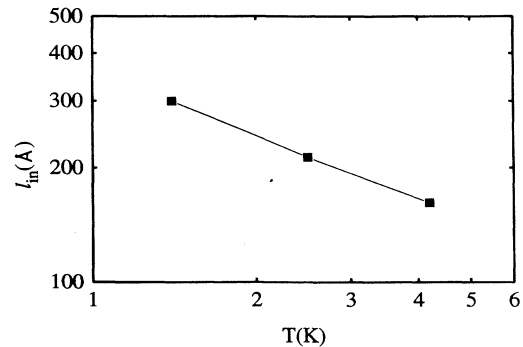

FIG. 7. Inelastic-scattering length (l_{in}) vs T for PANI-CSA in the metallic regime.

TRANSPORT IN POLYANILINE NEAR THE CRITICAL . . .

$(L_H/L_c)^{1/\eta}$, where c is the velocity of light. Because of this ability to shift E_c by an external magnetic field, one can envision a crossover from the critical behavior with a power-law dependence for $\rho(T)$ in zero field to insulating behavior with variable-range hopping among localized states. The Khmelnitskii-Larkin criterion for this crossover is the following:

$$L_H/L_c \sim 1 . \qquad (11)$$

In an earlier report, we demonstrated that it is possible to induce the crossover from the critical regime to variable-range hopping by application of an external magnetic field.[4] For $\eta = 3.8$ (●), the VRH plot for $H = 10$ T (◆) becomes approximately linear as shown in Fig. 8. However, since $\eta = 3.8$ for the data in Fig. 8, the system is just beyond the critical region on the metallic side. Thus, one would expect that an even stronger magnetic field would be required to achieve complete localization.

The $\ln(\rho(T,H)$ vs $T^{-1/4}$ plots for two samples with $\eta = 3.8$ (●) and $\eta = 2.8$ (■) are compared in Fig. 8. In both cases, high magnetic fields induce the crossover from power-law behavior to VRH. We find $T_0(H = 10$ T$) = 27$ K for the sample with $\eta = 3.8$ and T_0 $(H = 8$ T$) = 56$ K for the sample with $\eta = 2.8$.

The magnetoresistance (MR) for PANI-CSA in the critical and insulating regimes are shown in Figs. 9(a) and 9(b). In both regimes the MR is positive, but with larger values for the more disordered samples: at 1.4 K and $H = 8$ T, $\Delta\rho/\rho$ is 0.25 and 1.60 in the critical and insulating regimes, respectively. In both cases, the magnetoresistance is linear in H^2, up 8 T, at 4.2 K; however, for lower temperatures, the initial linear dependence is followed by saturation at higher fields. The qualitative features of the magnetoresistance are identical in the critical and insulating regimes, although the magnitude of the magnetoresistance increases dramatically as the system moves closer to the insulating regime. The positive magnetoresistance in the critical region $(\rho \propto T^{-0.26})$, as shown in Fig. 9(a), is enhanced by a factor of 2 with
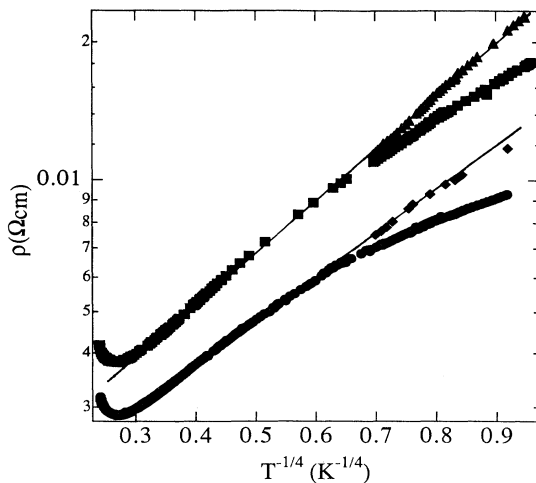

FIG. 8. $\rho(T)$ vs $T^{-1/4}$ for PANI-CSA in the critical regime: $[\rho(T) \propto T^{-0.26}]$, $H = 0$ T (●), and $H = 10$ T (◆); $[\rho(T) \propto T^{-0.36}]$, $H = 0$ T (■), and $H = 8$ T (▲).
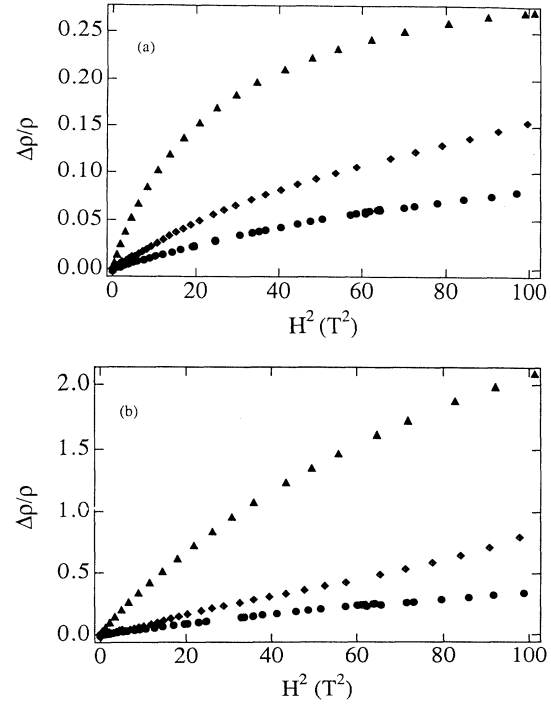

FIG. 9. $(\Delta\rho/\rho)$ vs H^2 for PANI-CSA: (a) In the critical regime; $[\rho(T) \propto T^{-0.26}]$, 4.2 K (●), 2.5 K (◆), and 1.4 K (▲); (b) in the insulating regime $(T_0 = 2.9 \times 10^4$ K), 4.2 K (●), 2.5 K (◆), and 1.4 K (▲).

respect to the samples in the metallic regime, since the magnetic field induces a transition from the critical regime to the insulating side of the MI transition.

The large positive magnetoresistance in the insulating regime (VRH with $T_0 = 2.9 \times 10^4$ K), as shown in Fig. 9(b) is typical of that expected for the VRH conduction mechanism.[24] Since the overlap of the localized state wave functions shrinks in the presence of magnetic field, the hopping length must correspondingly increase. Therefore, the VRH resistivity is strongly dependent on the strength of the magnetic field. The localization length can be independently estimated from the expression for the magnetic-field dependence of the VRH resistivity:[24]

$$\ln[\rho(H)/\rho(0)] = t \left[\frac{L_c}{L_H} \right]^4 \left[\frac{T_0}{T} \right]^{3/4} , \qquad (12)$$

where $t = (5/2016)$, L_H is the magnetic length, $\hbar$ is Planck's constant, c is the velocity of light, and e is the electron charge. As shown in Figs. 10(a) and 10(b) the plots of $\ln[\rho(H)/\rho(0)]$ vs $T^{-3/4}$ (at constant H) are consistent with Eq. (12). The localization lengths can be calculated from T_0 and the slopes of Figs. 10(a) and 10(b) by using Eq. (12). The use of Eq. (12) requires that the transport occurs via variable-range hopping among localized states, either for samples on the insulating side of the MI transition (where $\ln\rho$ vs $T^{-1/4}$ is a straight line in zero field) or for samples in the critical regime (where $\ln\rho$ vs $T^{-1/4}$ is a straight line only at high magnetic fields). For
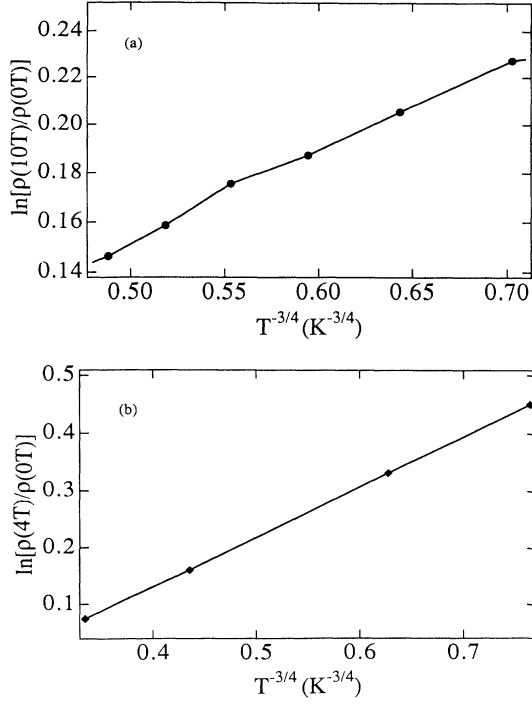
FIG. 10. $\ln[\rho(H)/\rho(0)]$ vs $T^{-3/4}$ for PANI-CSA: (a) In the critical regime $[\rho(T) \propto T^{-0.26}]$ at $H = 10$ T; (b) in the insulating $(T_0 = 2.9 \times 10^4$ K) regime at $H = 4$ T.

the sample in the critical regime in Fig. 1, the slope of the data (●) in Fig. 8 yields T_0 ($H = 10$ T) $= 27$ K and L_c ($H = 10$ T) ≈ 153 Å. For the sample in the insulating regime in Fig. 1, the slope of the $\ln\rho$ vs $T^{-1/4}$ plot in Fig. 3(a) yields $T_0 = 2.9 \times 10^4$ K, and L_c ($H = 4$ T) ≈ 80 Å. Thus even at $H = 10$ T, L_c for the sample in the critical regime is greater than L_c for the insulating sample, which shows the critical divergence of L_c at the MI transition.

Note that for $H = 10$ T, $L_H = 83$ Å. In both cases shown in Fig. 8, therefore, the magnetic-field-induced crossover into the VRH regime is consistent with the Khmelnitskii-Larkin criterion [Eq. (11)]. For the sample with $\eta = 3.8$, the crossover to the $T^{-1/4}$ dependence is not quite complete even at the 10-T field, whereas for $\eta = 2.8$, $H = 8$ T is sufficient to achieve straight-line behavior on a $\ln\rho$ vs $T^{-1/4}$ plot.

D. Temperature dependence of the thermoelectric power

The temperature dependence of thermoelectric power, $S(T)$, of PANI-CSA has been measured in the metallic, critical $(\rho \propto T^{-0.26})$, and insulating (VRH with $T_0 = 2.9 \times 10^4$ K) regimes.[9] The room-temperature value is approximately 10 μV/K with small variations (± 2 μV/K) depending on the details of the sample-casting process.[9] The magnitude and sign of $S(T)$ are similar to results obtained from a number of partially doped p-type conducting polymers.[25–27] The positive sign of the thermopower is consistent with the calculated band structure of the metallic emeraldine salt, having a three-quarter-filled π band with one hole per repeat unit

(-B-NH-B-NH-, where B denotes a phenyl ring in the benzenoid form).[28,29] The linear temperature dependence[9] of $S(T)$ corresponds to the characteristic diffusion thermopower of a metal, or alternatively can be interpreted as the entropy per carrier.

For a disordered system with a partially filled electronic band, there is a finite density of states at the Fermi energy. If the disorder is sufficiently weak that E_F lies in the regime of extended states, the temperature dependence can be expressed as follows:[30]

$$S = \frac{\pi^2}{3} \frac{k_B}{e} k_B T \left| \frac{d \ln\sigma(E)}{dE} \right|_{E_F}, \tag{13}$$

where the energy dependence of the conductivity, $\sigma(E)$, generally arises from both the band structure and the energy dependence of the mean scattering time. A relatively large magnitude of $S(T)$ in comparison with typical metals suggests that a relatively small bandwidth is responsible for the linear temperature dependence,[28,29] rather than an energy-dependent scattering process. If we assume that $\sigma(E)$ is a slowly varying function in the vicinity of E_F, Eq. (13) is equivalent to the free-electron approximation result,

$$S_m(T) = +(\pi^2/3)(k_B/|e|)k_B T(z/E_F), \tag{14}$$

where z is a constant (determined from the band structure and the energy dependence of the mean scattering time). The positive sign indicates that the π band is more than half filled. Using $z = 1$, $E_F \approx 1$ eV,[28,29] and $T = 300$ K, Eq. (8) yields S (300 K) ≈ 7.5 μV/K, close to the measured value. The density of states estimated from Eq. (14) is 1.1–1.6 states per eV per two rings, consistent with the value of 1 state per eV per two rings obtained from magnetic-susceptibility measurement.[6]

For PANI doped with conventional protonic acids, $S(T)$ follows a U-shaped temperature dependence with a negative sign for unoriented and fully protonated samples.[8,31] The positive and quasilinear dependence of $S(T)$ were observed only in oriented (tensile drawn) polyaniline films.[31] The absence of the linear temperature dependence for unorientated samples in previous studies is, evidently, due to the higher degree of disorder, the inhomogeneous distribution of dopant ions, and the formation of "metallic islands," all of which suppressed the intrinsic behavior. The thermopower of PANI-CSA (Ref. 9) is insensitive to the details of the temperature dependence of the resistivity. The linear dependence of the thermopower for all three regimes confirms the conclusion that PANI-CSA processed from solution in m-cresol is near the metal-insulator boundary.[9]

For variable-range-hopping transport, the thermopower can be written as S_{hop},[30]

$$S_{\text{hop}} = -\frac{1}{2} \frac{k_B}{|e|} \frac{W_s^2}{k_B T} \left| \frac{d \ln N(E)}{dE} \right|_{E_F}, \tag{15}$$

where for VRH, $W_s^2/k_B T = k(T_0 T)^{1/2}$. Thus, in the VRH regime, $S_{\text{hop}}(T)$ varies as $T^{1/2}$, tending to zero as T goes to zero. On the other hand, one expects a contribution to the thermopower like that in Eq. (14) even when

the Fermi energy lies in a region of localized states (since the entropy per carrier is determined by the low-energy excitations). Comparing the hopping term (S_{hop}) with metallic thermopower (S_m),

$$\left| \frac{S_{hop}}{S_m} \right| \propto \left[\frac{T_0}{T} \right]^{1/2} . \tag{16}$$

Thus, the hopping contribution to the thermopower would be expected to dominate the thermopower for $T \ll T_0$. The thermopower data shown in detail in Ref. 9 remain linear over the entire temperature range, even for the sample for which the resistivity follows the VRH temperature dependence at temperatures as low as $T < T_0 \approx 3 \times 10^4$ K. The linear temperature dependence of $S(T)$ implies therefore that the one-dimensional electronic structure of the PANI chains is very close to that of a metal, even in the VRH regime close to the MI transition.

IV. CONCLUSION

Three distinct and characteristic types of transport have been identified for PANI-CSA films from the reduced activation energy (W) versus temperature plots: transport on the metallic side of the MI transition, transport in the critical regime, and transport on the insulating side of the MI transition. In the metallic regime, the $T^{1/2}$ dependence of conductivity at low temperatures implies the contribution of the electron-electron interaction to conductivity and magnetoconductivity. The T^{-1} dependence of inelastic-scattering time (τ_{in}) is in agreement with the prediction for systems very near to the MI transition. The inelastic-scattering time (τ_{in}) of the order of 10^{-10} sec is typical of that of amorphous metals. In the critical regime near the Anderson MI transition, the power-law temperature dependence of $\rho(T)$ is in excellent agreement with the theory of Larkin and Khmelnitskii. Magnetic fields of 8–10 T induce a crossover from the critical regime into the insulating state where the states

near E_F are localized and the transport takes place via variable-range hopping. The typical localization length in PANI-CSA just on the insulating side of the MI transition (VRH transport begins to dominate) is about 80–130 Å. For PANI-CSA, the thermopower exhibits the linear temperature dependence characteristic of "metallic" behavior. The linear dependence is insensitive to the details of the resistivity; the "metallic" thermopower is characteristic of all samples studied with properties in the vicinity of the metal-insulator transition.

The demonstration that PANI-CSA cast from solution in m-cresol is on the boundary of the metal-insulator transition provides an important fixed point. Although improvement in material quality will quite generally improve electrical properties, reduction in disorder *within the metallic regime* will increase the mean free path for carriers in extended states. That this fixed point has been achieved in materials cast directly from solution without subsequent processing suggests that major improvements in electrical conductivity can be anticipated for polyaniline protonated with surfactant counterions. This is particularly important since the counterion-induced processibility provides an opportunity for further improvement of the structural order to achieve chain-extended and chain-aligned material in which the elastic scattering is sufficiently weak to allow true metallic behavior in three dimensions. In this limit, the room-temperature conductivity parallel to the chain direction has been previously estimated[4] to be greater than 10^4 S/cm.

[1]A. J. Heeger, S. Kivelson, J. R. Schrieffer, and W. P. Su, Rev. Mod. Phys. **60**, 781 (1988).

[2]A. B. Kaiser, Synth. Met. **45**, 183 (1991), and references therein.

[3]Yong Cao, Paul Smith, and Alan J. Heeger, Synth. Met. **48**, 91 (1992).

[4]M. Reghu, Y. Cao, D. Moses, and A. J. Heeger, Phys. Rev. B **47**, 1758 (1993).

[5]T. Ishiguro, H. Kaneko, Y. Nogami, H. Ishimoto, H. Nishiyama, J. Tsukamoto, A. Takahashi, M. Yamamura, T. Hagiwara, and K. Sato, Phys. Rev. Lett. **69**, 660 (1992).

[6]Y. Cao and A. J. Heeger, Synth. Met. **52**, 193 (1992).

[7]N. S. Sariciftci (private communication).

[8]F. Wudl, R. O. Angus, F. L. Lu, P. M. Allemand, D. J. Vachon, M. Nowak, Z. X. Liu, and A. J. Heeger, J. Am. Chem. Soc. **109**, 3677 (1987).

[9]C. O. Yoon, M. Reghu, D. Moses, A. J. Heeger, and Y. Cao, Phys. Rev. B **48**, 14 080 (1993).

[10]A. I. Larkin and D. E. Khmelnitskii, Zh. Eksp. Teor. Fiz. **83**,

1140 (1982) [Sov. Phys. JETP **56**, 647 (1982)].

[11]Y. W. Park, Synth. Met. **45**, 173 (1991); P. M. Chaikin and J. F. Kwak, Rev. Sci. Instrum. **46**, 218 (1975).

[12]R. B. Roberts, Philos. Mag. **36**, 91 (1977).

[13]A. G. Zabrodskii and K. N. Zeninova, Zh. Eksp. Teor. Fiz. **86**, 727 (1984) [Sov. Phys. JETP **59**, 425 (1984)].

[14]N. F. Mott and E. Davis, *Electronic Processes in Noncrystalline Materials* (Clarendon, Oxford, 1979).

[15]P. A. Lee and T. V. Ramakrishnan, Rev. Mod. Phys. **57**, 287 (1985).

[16]D. Belitz and K. I. Wysokinski, Phys. Rev. B **36**, 9333 (1987).

[17]Peihuya Dai, Youzhu Zhang, and M. P. Sarachik, Phys. Rev. B **45**, 3984 (1992); **46**, 6724 (1992).

[18]T. F. Rosenbaum, R. M. F. Milligan, G. A. Thomas, P. A. Lee, T. V. Ramakrishnan, and R. N. Bhatt, Phys. Rev. Lett. **47**, 1758 (1981).

[19]A. Kawabata, Solid State Commun. **34**, 431 (1980).

[20]S. Hikami, A. Larkin, and Y. Nagaoka, Prog. Theor. Phys. **63**, 707 (1980).

[21]G. Thummes, F. Korner, and J. Kotzler, Solid State Commun. **67**, 215 (1988).

[22]J. B. Beri, A. Fert, G. Creuzet, and A. Schul, J. Phys. F **16**, 2099 (1986).

[23]D. E. Khmelnitskii and A. I. Larkin, Solid State Commun. **39**, 1069 (1981).

[24]B. I. Shklovskii and A. L. Efros, *Electronic Properties of Doped Semiconductors* (Springer-Verlag, Berlin, 1984), p. 212; A. N. Ionov and I. S. Shlimak, in *Hopping Transport in Solids,* edited by M. Pollak and B. Shklovskii (North-Holland, Amsterdam, 1991), p. 377.

[25]Y. W. Park, A. J. Heeger, M. A. Druy, and A. G. MacDiarmid, J. Chem. Phys. **73**, 94 (1980); Y. W. Park, C. O. Yoon, C. H. Lee, H. Shirakawa, Y. Suezaki, and K. Akagi, Synth. Met.

28, D27 (1991).

[26]A. Watanabe, M. Tanaka, and J. Tanaka, Bull. Chem. Soc. Jpn. **54**, 2278 (1981).

[27]A. B. Kaiser, Phys. Rev. B **40**, 2806 (1989).

[28]D. S. Boudreaux, R. R. Chance, J. F. Wolf, L. W. Shacklette, J. L. Bredas, B. Thermans, J. M. Andre, and R. S. Silbey, J. Chem. Phys. **85**, 4584 (1986).

[29]S. Stäfstrom, J. L. Bredas, A. J. Epstein, H. S. Hoo, D. B. Tanner, W. S. Huang, and A. G. MacDiarmid, Phys. Rev. Lett. **59**, 1464 (1987).

[30]N. F. Mott, *Conduction in Non-Crystalline Materials* (Oxford University Press, Oxford, 1987).

[31]Z. H. Wang, E. M. Sherr, A. G. MacDiarmid, and A. J. Epstein, Phys. Rev. B **45**, 4190 (1992).